JOC The Journal of Organic Chemistry

Article

pubs.acs.org/joc

# Computational Studies on Reaction Mechanism and Origins of Selectivities in Nickel-Catalyzed (2 + 2 + 2) Cycloadditions and Alkenylative Cyclizations of 1,6-Ene−Allenes and Alkenes

Tao Yang*,†,‡ and Masahiro Ehara*,†,‡

†Institute for Molecular Science and Research Center for Computational Science, Nishigonaka 38, Myodaiji, Okazaki 444-8585, Japan

‡Elements Strategy Initiative for Catalysts and Batteries (ESICB), Kyoto University, Kyoto 615-8520, Japan

Supporting Information

**ABSTRACT:** The reaction mechanism and origins of ligand-controlled selectivity, regioselectivity, and stereoselectivity of Ni-catalyzed (2 + 2 + 2) cycloadditions and alkenylative cyclizations of 1,6-ene-allenes and alkenes were studied by using density functional theory. The catalytic cycle involves intermolecular oxidative coupling and an intramolecular concerted 1,4-addition step to afford a stable metallacycloheptane intermediate; these steps determine both the regioselectivity and stereoselectivity. Subsequent C−C reductive elimination leads to the cyclohexane product, whereas the *β*-hydride elimination leads to the *trans*-diene product. The selectivity between (2 + 2 + 2) cycloadditions and alkenylative cyclizations is controlled by the ligand. Irrespective of the nature of the terminal substituents on the ene−allene and alkene, the P(*o*-tol)$_3$ ligand always favors the C−C reductive elimination, resulting in the cyclohexane product. On the other hand, the flexibility of the PBu$_3$ ligand means that electronic and steric factors play important roles. Electron-withdrawing groups such as CO$_2$Me in the ene−allene terminal substituent induce obvious substrate−ligand repulsion and destabilize the C−C reductive elimination, giving rise to the *trans*-diene product.

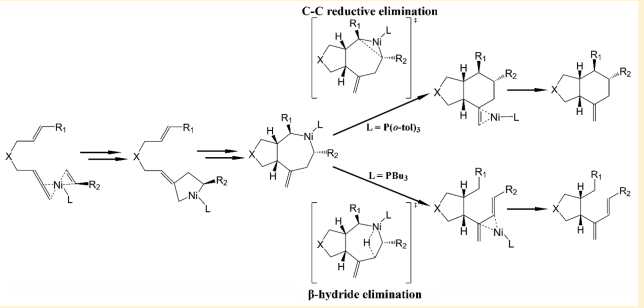


## INTRODUCTION

The design and discovery of new reactions that increase molecular complexity are an important goal in organic chemistry, and strategies that can be used to construct multiple bonds and stereogenic centers from simple chemical components in a single step have attracted broad interest.[1] In this respect, three-component (2 + 2 + 2) cycloaddition, which can be used to transform easily accessed *π* components into functionalized carbo- and heterocyclic systems in a one-step process, has become established as a prototypical example of such a strategy.[2] To date, various transition-metal catalysts have exhibited excellent catalytic activities toward (2 + 2 + 2) cycloadditions, including cobalt,[3] nickel,[4] ruthenium,[5] rhodium,[6] palladium,[7] and gold.[8] Although three *σ* bonds are constructed in all (2 + 2 + 2) cycloadditions, the number of generated stereogenic centers in this process depends completely on the nature of the *π*-systems involved. For example, the cyclotrimerization reaction with three alkynes delivers benzenoid systems that possess no stereocenter. On the other hand, an ideal (2 + 2 + 2) cycloaddition for increasing molecular complexity would use only alkenes and could theoretically provide access to cyclohexanes containing six contiguous stereocenters.

Since each alkyne reduces the number of stereocenters of a carbocyclic structure by two upon (2 + 2 + 2) cycloaddition, the stereochemical complexity of the carboncyclic product is intrinsically limited by the number of alkynes. To obtain highly complex carbocyclic structures, alkenes are gradually introduced as *π* components to replace alkynes. Significant progress has recently been made for transition-metal-catalyzed (2 + 2 + 2) cycloaddition involving multiple alkenes. In 1999, Montgomery reported a nickel-catalyzed intermolecular (2 + 2 + 2) cycloaddition of two enones and one alkyne.[4d] Recently, a regioselective (2 + 2 + 2) cycloaddition involving two alkenes and one alkyne, in which cationic rhodium was used as the catalyst, was reported by Tanaka et al.[9] Moreover, Pla-Quintana, Solà and co-workers studied a stereoselective Rh-catalyzed (2 + 2 + 2) cycloaddition of linear allene−ene/yne−allene substrates with both experimental and theoretical methods.[6d] Meanwhile, Alexanian's group disclosed that Rh(I)-catalyzed (2 + 2 + 2) cycloadditions of 1,6-ene−allenes and allenes deliver diastereo- and enantioselective *trans*-fused carbocycles with four stereocenters.[6f] Very recently, the same group reported stereoselective Ni-catalyzed (2 + 2 + 2) cycloadditions of 1,6-ene−allenes and alkenes, in which *cis*-fused carbocycles with up to five contiguous stereocenters were synthesized.[4b]

**Received:** December 10, 2016
**Published:** January 17, 2017

ACS Publications © 2017 American Chemical Society



DOI: 10.1021/acs.joc.6b02957
J. Org. Chem. 2017, 82, 2150−2159

**Scheme 1. Proposed Mechanisms for Ni-Catalyzed (2 + 2 + 2) Cycloadditions and Alkenylative Cyclizations**[4b]

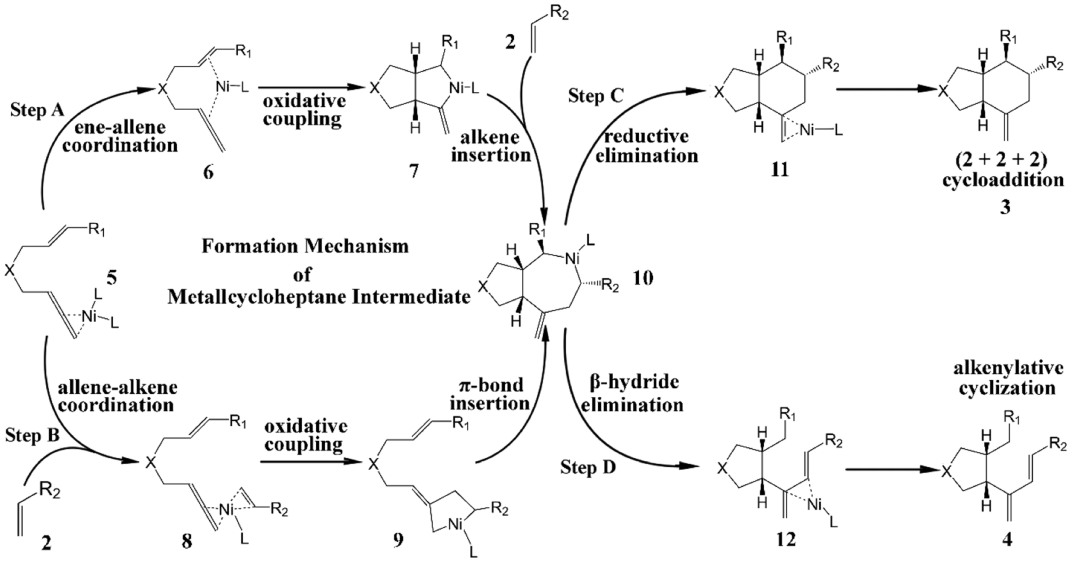


Even though transition-metal-catalyzed (2 + 2 + 2) cycloadditions involving ene−allenes are essential to attain six-numbered ring carbocycles with high stereochemical complexity, their reaction mechanism and selectivity remain unclear. In general, all these (2 + 2 + 2) cycloadditions are likely to occur via a metallacycloheptane intermediate (**10**, Scheme 1); however, two distinct plausible mechanisms of formation have been proposed.[4b,6c,g,9] Step **A** starts with an intramolecular oxidative coupling of the ene−allene substrate to form a metallacyclopentane intermediate **7** followed by intermolecular alkene (or allene) insertion. Step **B** involves an initial intermolecular oxidative coupling of ene−allene and alkene (or allene) to generate a metallacyclopentane intermediate **9**. Given that carbocycles with high numbers of stereocenters are widely found in biological and pharmaceutical compounds, answering the question of whether the intramolecular or intermolecular oxidative coupling is the initial step will provide a deeper understanding of the reaction mechanism and selectivity in (2 + 2 + 2) cycloadditions. This would have an impact on the synthetic utility of these cycloadditions, and could ultimately lead to the ideal reaction involving (2 + 2 + 2) cycloadditions with three alkenes.

In subsequent steps after formation of the metallacycloheptane intermediate, the metal catalyst has a remarkable influence on the mechanism and thereby determines the structure of the final product. The Rh-catalyzed reactions of 1,6-ene-allenes and alkenes always follow (2 + 2 + 2) cycloadditions to afford cycloadducts, irrespective of the metal ligands used.[6c,f] In contrast, nickel shows strong ligand control in the selectivity of the (2 + 2 + 2) cycloadduct and the alkenylative cyclization product,[4b] which corresponds to the tendency to undergo C−C reductive elimination and *β*-hydride elimination steps after formation of the metallacycloheptane intermediate. As shown in Scheme 2, reaction with the P(*o*-tol)$_3$ ligand always delivers a *cis*-hydrinane **3** through reductive elimination, whereas with PBu$_3$ as ligand, alkenylative cyclization occurs directly to produce *trans*-diene product **4** through *β*-hydride elimination.

In the present study, we performed comprehensive density functional theory (DFT) calculations[10] on Ni-catalyzed (2 + 2 + 2) cycloadditions and alkenylative cyclizations of 1,6-ene-allenes and alkenes to better understand the reaction

**Scheme 2. Ni-Catalyzed Intermolecular (2 + 2 + 2) Cycloaddition and Alkenylative Cyclization of 1,6-Ene−Allenes and Alkenes**

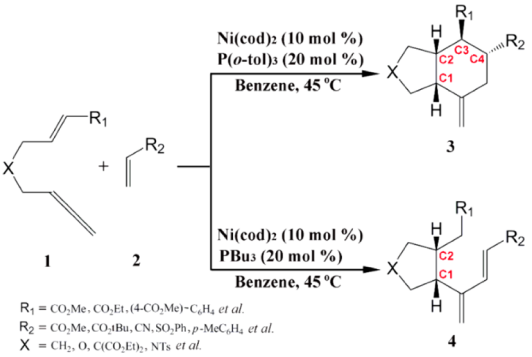


mechanism and to analyze the origins of ligand-controlled selectivity, regioselectivity, and stereoselectivity. By investigating competing pathways in the formation mechanism of the metallacycloheptane intermediate and two diverse products, catalytic cycles of both (2 + 2 + 2) cycloaddition and alkenylative cyclization are presented by using Ni(PMe$_3$)$_2$ as a catalyst model. The origins of ligand and substitution effects on the selectivity are then discussed with various ene−allenes and alkenes by using the experimentally applied ligands Ni(PBu$_3$)$_2$ and Ni(P(*o*-tol)$_3$)$_2$.

## COMPUTATIONAL METHODS

Geometry optimizations of all reactants, intermediates, transition states (TSs), and products were performed with the hybrid density functional B3LYP[11] in the gas phase. The effective core potential (ECP) with the corresponding double-*ξ* valence basis set (Lanl2dz)[12] was used to describe Ni while the all-electron basis set 6-31G(d,p) was used for all other atoms. Test optimizations by using M06,[13] BP86,[11c,14] *ω*B97XD,[15] and B2PLYPD[16] functionals gave similar geometries to those obtained with B3LYP (see the Supporting Information). Frequency calculations were carried out at the same level of theory to confirm all optimized structures are local minima or have one (and only one) imaginary frequency. To evaluate electronic energies, single-point energy calculations at the M06 level with SDD[17] ECP and the basis set for Ni and the 6-311++G(2d,2p) basis set for all other elements were performed on the gas-phase optimized geo-



DOI: 10.1021/acs.joc.6b02957
J. Org. Chem. 2017, 82, 2150−2159

metries. Solvation free energy corrections were calculated by using the SMD model[18] with benzene as the solvent for consistency with the experiment. Gibbs free energies reported below include zero-point vibrational energy corrections, thermal corrections at 298 K and 1 atm, and solvation free energy corrections. The B3LYP-D3 (Becke-Johnson damping, BJ),[19] B2PLYPD, and mPW2PLYPD[16,20] with the same basis sets were also tested for single-point energy calculations, which gave similar results (see the Supporting Information for details). The electron charge states were obtained from natural bond orbital (NBO)[21] analysis at the M06/SDD-6-311++G(2d,2p)-SMD-(benzene) level. All DFT calculations were carried out with Gaussian 09.[22] Molecular structures were illustrated with CYLView.[23]

## RESULTS AND DISCUSSION

Given the large size of the substrates and ligands used in Alexanian's experiments,[4b] 1,6-ene-allene **14** and alkene **16** along with Ni(0)/$PMe_3$ were used as a model. Although the reaction of ene−allene **14** and alkene **16** was not performed in Alexanian's experiments, this is considered to be a suitable model to clarify possible competing pathways of catalytic cycles.

**Formation Mechanism of the Metallocycloheptane Intermediate.** Possible pathways of the formation mechanism of a metallocycloheptane intermediate **23** from the ene−allene **14** and alkene **16** are calculated and summarized in Figure 1.

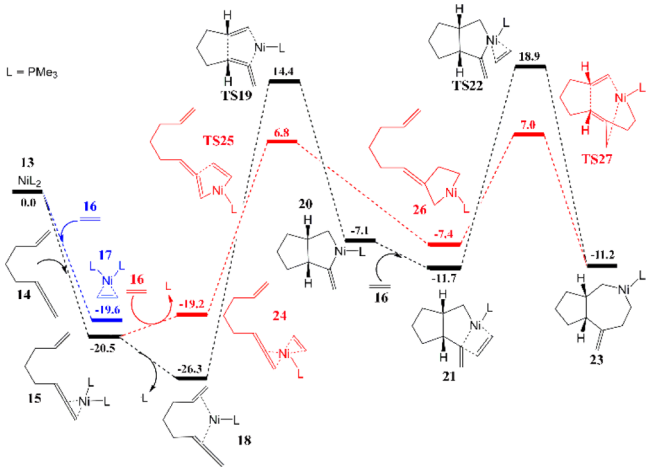


**Figure 1.** Energy diagram with Gibbs free energies (in kcal/mol) of [Ni($PMe_3$)$_2$]-catalyzed formation mechanism of the metallcycloheptane intermediate.[24]

Optimized structures of selected intermediates and transition states are presented in Figures 2 and 3. It has been revealed in previous studies that the catalyst Ni($PMe_3$)$_2$ initially forms a $\pi$-complex with substrates such as alkenes, alkynes, and allenes.[25] Two different stable $\pi$-complexes were found, ene−allene-(bisphosphane)−nickel(0) complex **15** and alkene-(bisphosphane)−nickel(0) complex **17**. The former is predicted to be 0.9 kcal/mol more stable in energy than the latter, suggesting that **15** should be regarded as the initial $\pi$-complex. To obtain the metallocycloheptane intermediate **23**, one C−C bond and two Ni−C bonds are necessary to be formed. The order of these bond formation steps along with the alkene insertion step determines whether the oxidative coupling mechanism via the metallacyclopentene intermediate **20** or **26** is involved.

On the one hand, an intramolecular complexation takes place initially by replacing one phosphine with the intramolecular $\pi$-bond, giving complex **18** (−26.3 kcal/mol). Complex **18**

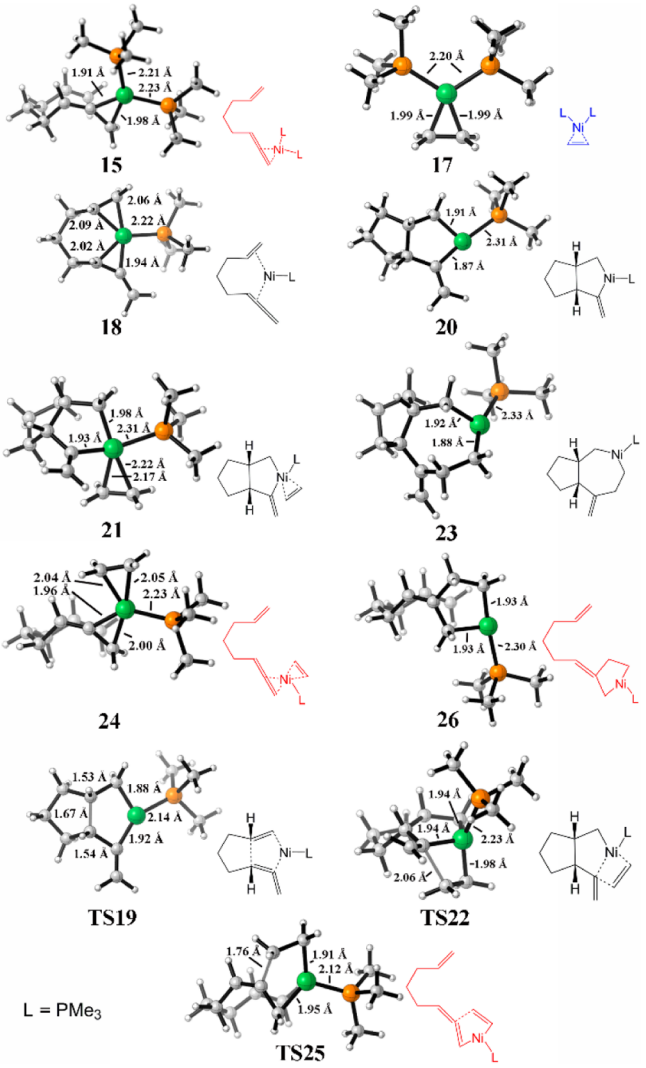


**Figure 2.** Optimized structures and significant bond distances of selected intermediates and transition states shown in Figure 1.

undergoes intramolecular oxidative coupling via **TS19**,[26] which is 14.4 kcal/mol higher in energy with respect to the isolated reactants, leading to metallacyclopentene intermediate **20**. Alkene **16** is then introduced to **20** by forming complex **21**. Through transition state **TS22**, with an energy barrier of 30.6 kcal/mol, alkene **16** is inserted and the stable metallacycloheptane intermediate **23** is formed, which is −11.2 kcal/mol in energy. The rate-determining step of this pathway is the alkene insertion step involving **TS22**, with an energy barrier of 45.2 kcal/mol (**18** to **TS22**).[27] Previous studies showed that the intramolecular oxidative couplings of alkyne−alkene and alkyne−alkyne usually have much lower barriers,[6d,e,28] whereas the calculations disclosed herein show that the alkene−alkene oxidative coupling may require more energy.

On the other hand, one phosphine of complex **15** is replaced through intermolecular complexation with **16**, resulting in the formation of complex **24** (−19.2 kcal/mol). The intermolecular oxidative coupling occurs via transition state **TS25**,[29] with a 27.3 kcal/mol barrier (**15** to **TS25**),[27] and formed metallacyclopentene intermediate **26**. A subsequent concerted 1,4-addition via six-membered cyclic transition state **TS27**, with a low barrier of 14.4 kcal/mol, gives rise to a metallacycloheptane intermediate **23**. The transition states that lead to three


DOI: 10.1021/acs.joc.6b02957
J. Org. Chem. 2017, 82, 2150−2159

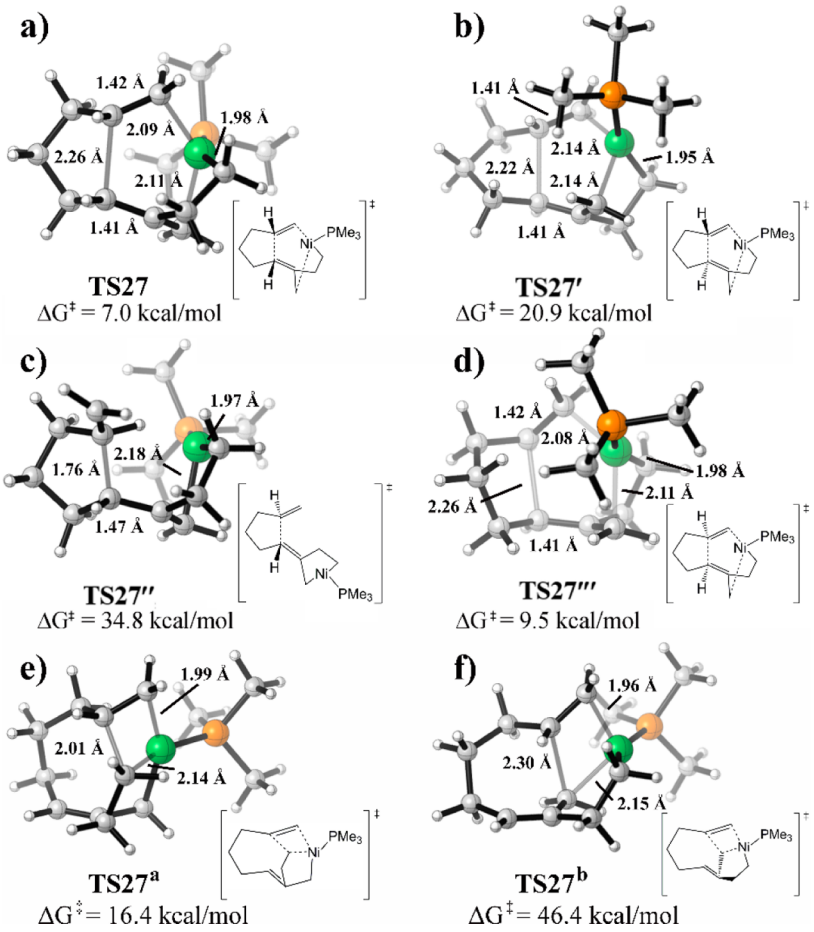


**Figure 3.** Possible transition states of the intramolecular oxidative coupling. (a–d) Four six-membered cyclic TSs which lead to different enantisomers of **23**; (e and d) four-membered migratory insertion TSs.

stereoisomers of the intermediate **23** were also located as **TS27′**, **TS27″**, and **TS27‴** (Figure 3), but they are clearly disfavored by at least 2.5 kcal/mol. This result is consistent with experimental observations which reveal that only products with the same stereocenters as found in **23** were synthesized. The classical four-membered alkene-insertion transition states were also located as **TS27**$^{a}$ and **TS27**$^{b}$, the energies of which are obviously higher than that of **TS27** (Figure 3). Recently, Himo et al. theoretically investigated the Rh-catalyzed 1:2 coupling of aldehydes and allenes and found that a similar six-membered cyclic TS is favored over the four-membered insertion TS in the formation of the second C–C bond.[30] As a result, the preferred pathway toward metallacycloheptane intermediate **23** is initial intermolecular oxidative coupling followed by an intramolecular concerted 1,4-addition step.[31]

**Formation Mechanism of (2 + 2 + 2) Cycloaddition and Alkenylative Cyclization Products.** From the metallocycloheptane intermediate **23** (−11.2 kcal/mol with respect to the isolated reactants), there are two different pathways: the C–C reductive elimination and the *β*-hydride elimination. The direct C–C reductive elimination takes place via transition state **TS28** (−7.8 kcal/mol), leading to the cyclohexane product **29** (−51.1 kcal/mol) (see Figure 4 and Figure 5). **29** ejects the carbocyle product **30** and regenerates the Ni(0) species. The energy barrier of cyclohexane generation is only 3.4 kcal/mol. In the case of the *β*-hydride elimination, the intermediate **23** initially undergoes a *β*-hydride transfer via a transition state **TS31** with a 11.2 kcal/mol barrier, forming a tetracoordinated

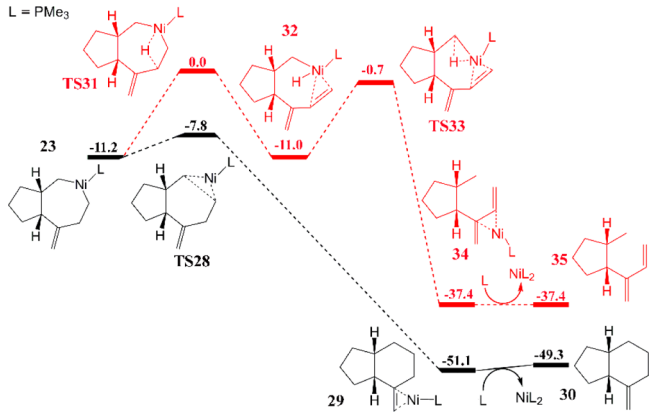


**Figure 4.** Energy diagram with Gibbs free energies (in kcal/mol) of $[Ni(PMe_3)_2]$-catalyzed (2 + 2 + 2) cycloaddition and alkenylative cyclization reactions from the metallcycloheptane intermediate. The (2 + 2 + 2) cycloaddition pathway is shown in black, and the alkenylative cyclization pathway is shown in red.

nickel(II) hydride complex **32** (−11.0 kcal/mol).[32] Subsequent C–H reductive elimination occurs through a transition state **TS33** which is 10.3 kcal/mol higher in energy than **32**, resulting in the product **34**. Finally, the alkenylative cyclization product **35** forms by regenerating the Ni(0) species. Further calculations with the experimentally used P(*o*-tol)$_3$ and PBu$_3$ ligands also confirmed that **TS31** has a higher energy barrier than **TS33**. Consequently, **TS28** and **TS31** which correspond


DOI: 10.1021/acs.joc.6b02957
J. Org. Chem. 2017, 82, 2150–2159

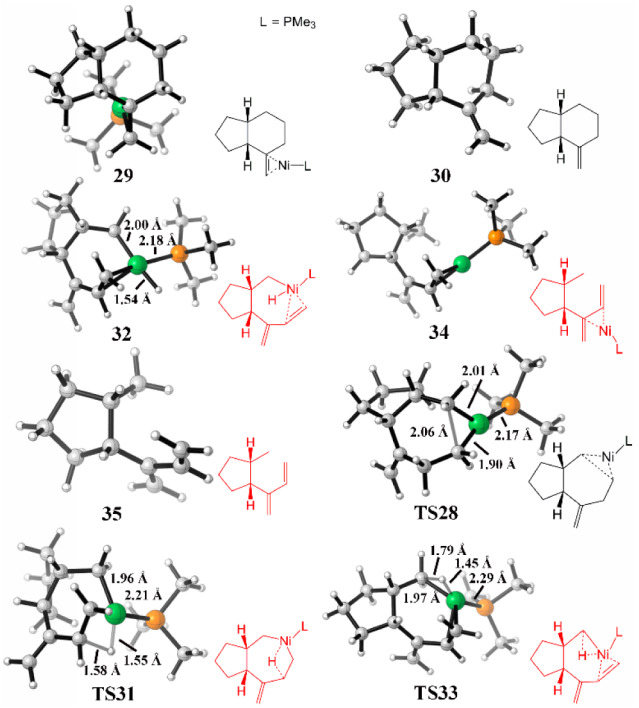


**Figure 5.** Optimized structures and significant bond distances of selected intermediates and transition states shown in Figure 4.

to the C−C reductive elimination and $\beta$-hydride elimination pathways, respectively, are the selectivity-determining steps for (2 + 2 + 2) cycloadditions and alkenylative cyclizations.

**Origins of Regioselectivities and Stereoselectivities of (2 + 2 + 2) Cycloadditions and Alkenylative Cyclizations.** As shown in Scheme 2, there are at least four stereocenters for (2 + 2 + 2) cycloaddition products and two stereocenters for alkenylative cyclization products, which are marked as stereocenter C1, C2, C3, and C4. The preferential formation of stereocenters C1 and C2 has been well explained by the lower energy of **TS27** over **TS27′**, **TS27″**, and **TS27‴**. When a substituent is introduced to $R_1$, the $\pi$-bond of 1,6-ene−allene possesses the *cis*-configuration, giving the (2 + 2 + 2) cycloaddition product with the $R_1$ in stereocenter C3 and the H in stereocenter C2 in a *syn* conformation, which is consistent with experimental observations. The formation of stereocenter C4, which is relative to the substituent $R_2$, will be discussed here.

The stereochemistry of stereocenter **4** is influenced by the intermolecular oxidative coupling step via **TS25** as presented in Figure 1. When a substituent is present at $R_2$, there are four possible pathways for the intermolecular oxidative coupling step, leading to diverse cyclohexanes and dienes, as shown in Table 1. However, only products **3-A** and **4-A** were observed experimentally. First, the substituent $CO_2Me$ is introduced as $R_2$ with $R_1$ = H, which is named reaction system **b**. The calculations for four different transition states with the $PMe_3$ ligand revealed that **TS25-A/B-*b*-PMe$_3$** have much lower energy barriers compared with **TS25-C/D-*b*-PMe$_3$**. More importantly, by introducing the substituent into $R_2$, the energy barrier of **TS25**, which is the rate-determining step of the full catalytic cycle, reduces dramatically from 27.3 kcal/mol to about 20 kcal/mol, indicating that these reactions occur smoothly under the experimental conditions. The reduction in the energy barriers of the intermolecular oxidative coupling stems from the fact that electron-withdrawing groups such as $CO_2Me$ lower the lowest-unoccupied molecular orbital (LUMO) of the alkene $\pi$-bond, which has been found in previous studies.[5f,33]

The preference of **TS25-A/B-*b*-PMe$_3$** over **TS25-C/D-*b*-PMe$_3$** is explained by the fact that electron-withdrawing groups such as $CO_2Me$ at the $\alpha$ position can stabilize the partial negative charge building upon the $\alpha$ carbon in the oxidative coupling step, which has been well explained by Stockis and

**Table 1. Computed Stereoselectivities in (2 + 2 + 2) Cycloadditions and Alkenylative Cyclizations of Ene−Allenes and Alkenes with PMe$_3$, P(*o*-tol)$_3$, and PBu$_3$ Ligands**

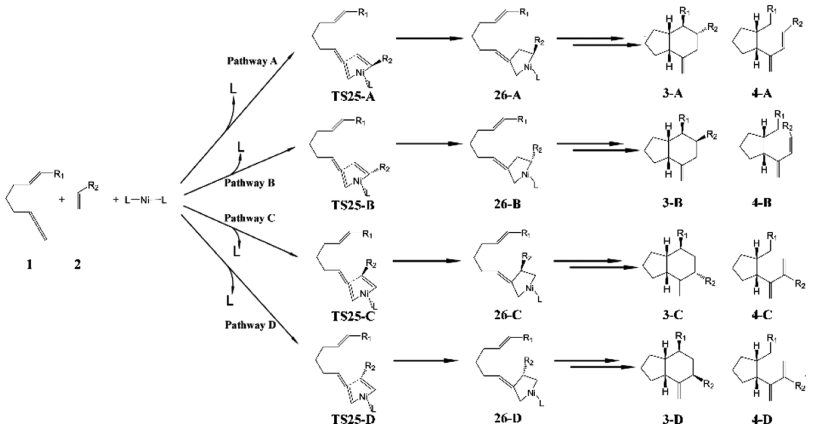


| | | | | energy barriers (kcal/mol) | | | | relative energy (kcal/mol) **TS27-A** is taken as reference | | | |
|---|---|---|---|---|---|---|---|---|---|---|---|
| system | $R_1$ | $R_2$ | ligand | **TS25-A** | **TS25-B** | **TS25-C** | **TS25-D** | **TS27-A** | **TS27′-A** | **TS27″-A** | **TS27‴-A** |
| **b** | H | $CO_2Me$ | $PMe_3$ | 20.9 | 20.1 | 32.8 | 36.4 | 0.0 | 5.7 | 32.7 | 2.2 |
| | H | $CO_2Me$ | P(*o*-tol)$_3$ | 19.8 | 17.0 | – | – | 0.0 | – | – | 5.2 |
| | H | $CO_2Me$ | $PBu_3$ | 16.3 | 16.8 | – | – | 0.0 | – | – | 2.4 |
| **d** | $CO_2Me$ | $CO_2Me$ | P(*o*-tol)$_3$ | 23.0 | 52.2 | – | – | 0.0 | – | – | 8.8 |
| | $CO_2Me$ | $CO_2Me$ | $PBu_3$ | 22.7 | 52.1 | – | – | 0.0 | – | – | 12.0 |



DOI: 10.1021/acs.joc.6b02957
J. Org. Chem. 2017, 82, 2150−2159

Hoffmann.[34] To analyze steric factors that stabilize **TS25-A/B-*b*-PMe$_3$**, the distortion/interaction model[25a,35] is introduced for the intermolecular oxidative coupling transition states of the reaction system **b** with the $PMe_3$ ligand. The distortion energy, $E_{dis}$, is defined as the energy needed to distort the ene−allene and alkene from their ground-state to transition-state geometries. As depicted in Figure 6, there is some correlation between distortion energies $E_{dis}^{\ddagger}$(substrate) and energy barriers for the four transition states. **TS25-A/B-*b*-PMe$_3$** have low energy barriers as well as small distortion energies, whereas, in the case of **TS25-C/D-*b*-PMe$_3$**, the energy barriers and distortion energies are clearly higher. Both electronic and steric factors favor the selectivity of **TS25-A/B-*b*-PMe$_3$**. Given the low energy barriers of **TS25-A-*b*-PMe$_3$** and **TS25-B-*b*-PMe$_3$**, we will focus on only **TS25-A** and **TS25-B**.

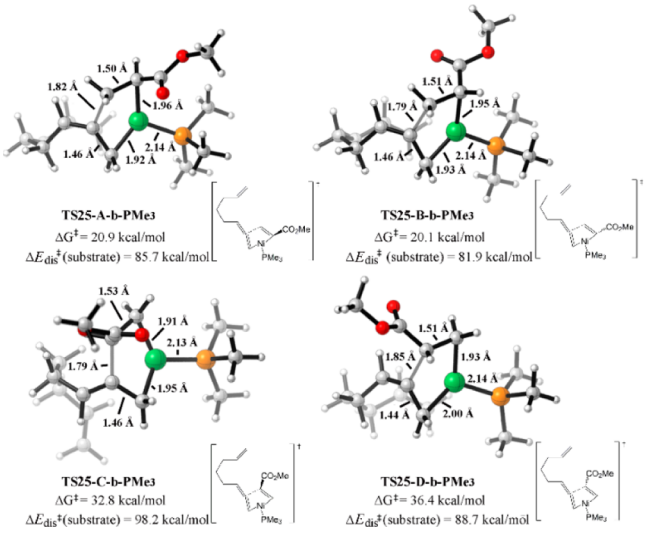


**Figure 6.** Optimized transition structures of **TS25** (oxidative coupling step) with the $PMe_3$ ligand for the reaction system **b** ($R_1$ = H and $R_2$ = $CO_2Me$).

The ligand change from $PMe_3$ to P(*o*-tol)$_3$ or $PBu_3$ still results in competitive energies of **TS25-A** and **TS25-B**, which is consistent with the experimental observation that cyclohexane diastereomers were obtained when $R_1$ = H.[4b] The experimentally used substituent $CO_2Me$ is introduced to $R_1$ with $R_2$ = $CO_2Me$ (reaction system **d**) to further delineate the stereoselectivity. It is found that irrespective of whether the ligand is P(*o*-tol)$_3$ or $PBu_3$, **TS25-A** presents an energy barrier of approximately 23 kcal/mol, whereas **TS25-B** is highly disfavored by at least 20 kcal/mol, in agreement with the experimental results. The significant increase in the energy barrier for the pathway proceeding via **TS25-B** for reaction system **d** is ascribed to steric crowding between $R_1$ = $CO_2Me$ and $R_2$ = $CO_2Me$, which leads to significant deformation of the TS geometries.

Because **26-A** may undergo rapid interconversion with **26-B** or its enantiomer through rotation of the tether, the six-membered cyclic transition state **TS27** also influences the diastereoselectivity between **3A** and **3B**. To further confirm that **24-A** will lead to **3A** (or **4A**) rather than **3B** (or **4B**), four possible six-membered cyclic **TS27-A**, **TS27′-A**, **TS27″-A**, and **TS27‴-A** based on **26A** were calculated. As presented in Table 1, with $PMe_3$, the introduction of $R_2$ = $CO_2Me$ does not change the order of four possible TSs and **TS27-A-*b*-PMe$_3$** has the lowest energy followed by **TS27‴-A-*b*-PMe$_3$**. Further calculations on reaction systems **b** and **d** with $Pbu_3$ and P(*o*-tol)$_3$ ligands confirmed that **TS27** is preferred over **TS27‴**. The above discussion revealed that the stereoselectivity at stereo-

**Table 2. Computed Selectivities between (2 + 2 + 2) Cycloaddition and Alkenylative Cyclization of Ene−Allenes and Alkenes with $PMe_3$, P(*o*-tol)$_3$, and $PBu_3$ Ligands**

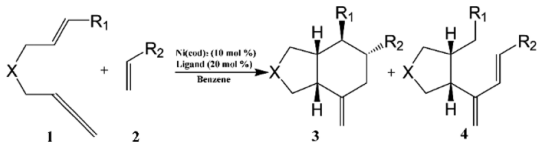


| reaction system | $R_1$ | $R_2$ | X | ligand | $\Delta\Delta G^{\ddagger}$(3−4) (kcal/mol) | major product | exp. selectivity (3:4) |
|---|---|---|---|---|---|---|---|
| **a** | H | H | $CH_2$ | $PMe_3$ | −7.8 | **3a** | |
| | H | H | $CH_2$ | P(*o*-tol)$_3$ | −15.7 | **3a** | |
| | H | H | $CH_2$ | $PBu_3$ | −8.7 | **3a** | |
| **b** | H | $CO_2Me$ | $CH_2$ | P(*o*-tol)$_3$ | −12.1 | **3b** | |
| | H | $CO_2Me$ | $CH_2$ | $PBu_3$ | −6.1 | **3b** | |
| **c** | $CO_2Me$ | H | $CH_2$ | P(*o*-tol)$_3$ | −7.4 | **3c** | |
| | $CO_2Me$ | H | $CH_2$ | $PBu_3$ | 0.3 | **4c** | |
| **d** | $CO_2Me$ | $CO_2Me$ | $CH_2$ | P(*o*-tol)$_3$ | −1.5 | **3d** | |
| | $CO_2Me$ | $CO_2Me$ | $CH_2$ | $PBu_3$ | 1.5 | **4d** | |
| **e** | $CO_2Me$ | $CO_2tBu$ | $CH_2$ | P(*o*-tol)$_3$ | −1.1 | **3e** | |
| | $CO_2Me$ | $CO_2tBu$ | $CH_2$ | $PBu_3$ | 4.0 | **4e** | |
| **f** | $CO_2Me$ | $CO_2tBu$ | $C(CO_2Et)_2$ | P(*o*-tol)$_3$ | −2.5 | **3f** | 100:0 |
| | $CO_2Me$ | $CO_2tBu$ | $C(CO_2Et)_2$ | $PBu_3$ | 3.2 | **4f** | 0:100 |
| **g** | $CO_2Et$ | $CO_2tBu$ | O | P(*o*-tol)$_3$ | −3.2 | **3g** | 100:0 |
| | $CO_2Et$ | $CO_2tBu$ | O | $PBu_3$ | 4.2 | **4g** | 0:100 |
| **h** | $CO_2Me$ | $CO_2Me$ | $C(CO_2Et)_2$ | P(*o*-tol)$_3$ | −0.9 | **3h** | 100:0 |
| **i** | $CO_2Me$ | $SO_2Ph$ | $C(CO_2Et)_2$ | P(*o*-tol)$_3$ | −0.6 | **3i** | 100:0 |
| **j** | $CO_2Me$ | CN | $C(CO_2Et)_2$ | $PBu_3$ | 3.2 | **4j** | 0:100 |
| **k** | $CO_2Me$ | *p*-$MeC_6H_4$ | $C(CO_2Et)_2$ | $PBu_3$ | 10.7 | **4k** | 0:100 |



DOI: 10.1021/acs.joc.6b02957
J. Org. Chem. 2017, 82, 2150−2159

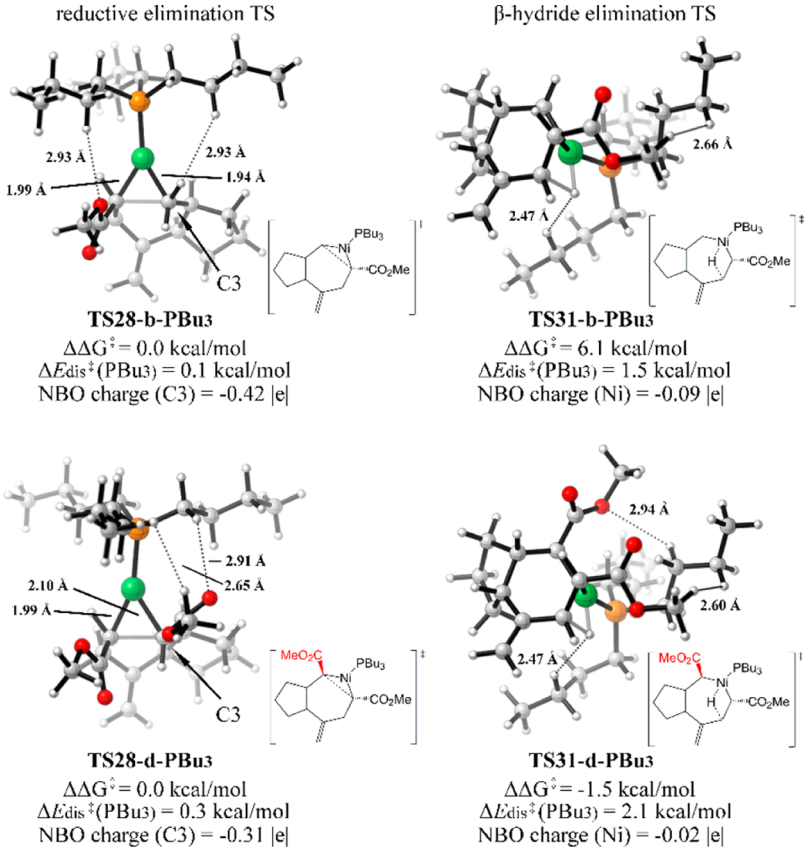


**Figure 7.** Optimized transition structures of **TS28** (reductive elimination in the (2 + 2 + 2) pathway) and **TS31** (*β*-hydride elimination in the alkenylative cyclization reaction) with the $PBu_3$ ligand for the reaction systems **b** ($R_1$ = H and $R_2$ = $CO_2Me$) and **d** ($R_1$ = $CO_2Me$ and $R_2$ = $CO_2Me$).

center C4 is significantly influenced by substituent $R_1$ rather than substituent $R_2$.

**Ligand Effects on Chemoselectivities between (2 + 2 + 2) Cycloadditions and Alkenylative Cyclizations.** When the P(*o*-tol)$_3$ ligand was employed experimentally, the (2 + 2 + 2) cycloaddition was preferred over the alkenylative cyclization reaction. However, compared with the P(*o*-tol)$_3$ ligand, the reaction with the $PBu_3$ ligand gave reversed selectivity and formation of the alkenylative carbocyclization product was favored. As depicted in Figure 4, the selectivity of formation of cyclohexane product **3** and alkenylative carbocyclization product **4** is determined by the energy difference between the transition states for C−C reductive elimination **TS28** and *β*-hydride elimination **TS31**. The energy differences between **TS28** and **TS31** and the predicted selectivity of the reaction systems with various substituents were computed and are given in Table 2. The predicted selectivities are in excellent agreement with the experimental data, where available. By comparing the energy difference between **TS28** and **TS31** of the reaction systems **e** and **f** by using P(*o*-tol)$_3$ and $PBu_3$ ligands, it is found that the tether has little influence on the selectivity. In fact, the activation energy for a given transition state changes less than 2 kcal/mol when the tether X changes from $CH_2$ to $C(CO_2Et)_2$. This result is similar to the results of a previous study on Ni-catalyzed (5 + 2) cycloaddition.[28b]

For the $PBu_3$ ligand, the preference for the formation of **3** and **4** depends on the terminal substituent $R_1$ in ene−allenes. When the substituent $R_1$ is a hydrogen atom, the major product is cyclohexane **3**, whereas diene **4** is formed with a bulky substituent such as $CO_2Me$ or $CO_2Et$ as $R_1$. To reveal the key role of substituent $R_1$, transition states of reaction systems **b** ($R_1$ = H and $R_2$ = $CO_2Me$) and **d** ($R_1$ = $CO_2Me$ and $R_2$ = $CO_2Me$) with the $PBu_3$ ligand are shown in Figure 7. For each reaction system, both the C−C reductive elimination transition state (**TS28**) leading to the (2 + 2 + 2) cycloaddition product and *β*-hydride elimination transition state (**TS31**) leading to the alkenylative cyclization product are depicted.

The $PBu_3$ ligand in **TS28** has $C_{3v}$ symmetry. The repulsive interaction between the substrate and ligand is slight, which is reflected in the long H−H distances. In the case of **TS31**, the $PBu_3$ ligand configuration changes to $C_{2v}$ by rotating one butyl group, to avoid the substrate−ligand repulsive interaction. To measure the energy change of the $PBu_3$ ligand, the ligand distortion energy $\Delta E_{dis}^{\ddagger}$(ligand), which is defined as the energy needed to distort $PBu_3$ from the ground state to the geometry in the transition state, is introduced. As presented in Figure 7, the $\Delta E_{dis}^{\ddagger}(PBu_3)$ for **TS28** is very small, whereas **TS32** has a higher $\Delta E_{dis}^{\ddagger}(PBu_3)$ ranging from 1.5 to 2.1 kcal/mol. Unexpectedly, although the presence of $CO_2Me$ as substituent $R_1$ increases the distortion energy by 0.6 kcal/mol, **TS31-d-PBu$_3$** becomes preferred over **TS28-d-PBu$_3$**, indicating that ligand distortion energy is not the only determining factor affecting the selectivity between **TS28** and **TS31**.

In fact, the preference of **TS31-d-Pbu$_3$** over **TS28-d-Pbu$_3$** can be mainly ascribed to the increment of the energy barrier of **TS28-d-Pbu$_3$**. Although the substrate−ligand interaction is not important in **TS28-PBu$_3$**, the presence of $R_1$ = $CO_2Me$ results in significant repulsion between the $R_1$ substituent and Ni and thereby increases the energy barrier. As shown in Figure 7, the Ni−C bond length increases from 1.94 Å in **TS28-*b*-Pbu$_3$** to


DOI: 10.1021/acs.joc.6b02957
J. Org. Chem. 2017, 82, 2150−2159

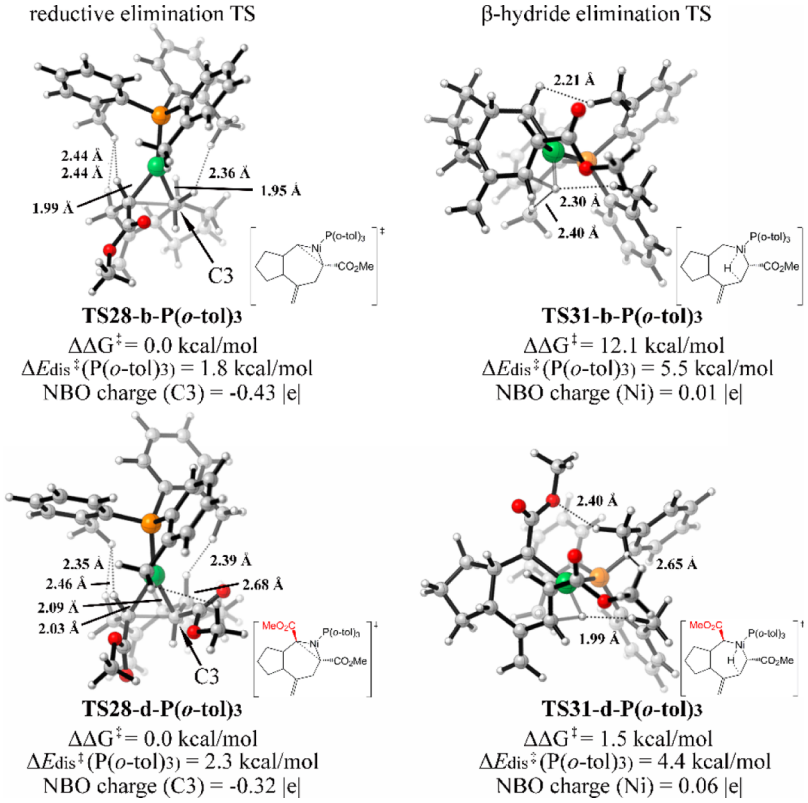


**Figure 8.** Optimized transition-state structures of **TS28** (reductive elimination in the (2 + 2 + 2) pathway) and **TS31** (*β*-hydride elimination in the alkenylative cyclization reaction) with the P(*o*-tol)$_3$ ligand for the reaction systems b ($R_1$ = H and $R_2$ = $CO_2Me$) and **d** ($R_1$ = $CO_2Me$ and $R_2$ = $CO_2Me$).

2.10 Å in **TS28-d-PBu$_3$**. Furthermore, because $R_1$ = $CO_2Me$, the NBO charge of C3 in **TS28** reduces from −0.42|e| to −0.31|e|, which also moderately disfavors the C−C reductive elimination. On the other hand, it is well-known that, in *β*-hydride elimination, a hydridic H atom is transferred from the *β* carbon to the metal center.[36] However, the NBO charge of Ni does not change much because there is no conjugation between $R_1$ = $CO_2Me$ and Ni. The above discussion reveals that the selectivity of the (2 + 2 + 2) cycloaddition and the alkenylative cyclization with the $PBu_3$ ligand is determined by both electronic and steric factors.

Compared with the $PBu_3$ ligand, the reaction with the P(*o*-tol)$_3$ ligand gives the reverse selectivity and always produces cyclohexane **3**. For example, in the reaction with $PBu_3$ ligand, the *β*-hydride elimination transition state **TS31-f-PBu$_3$** is favored by 3.2 kcal/mol, giving rise to the alkenylative cyclization product **4f**, whereas the reductive elimination transition state **TS28-f-P(*o*-tol)$_3$** is 2.5 kcal/mol lower in energy than *β*-hydride elimination transition state **TS31-f-P(*o*-tol)$_3$**, leading to the (2 + 2 + 2) cycloadduct **3f**. Again, reaction systems **b** and **d** are taken as examples to show the effect of the P(*o*-tol)$_3$ ligand. The optimized transition-state structures involved in the reductive elimination and the *β*-hydride elimination with the P(*o*-tol)$_3$ ligand are depicted in Figure 8.

In both the reductive elimination transition state (**TS28-P(*o*-tol)$_3$**) and the *β*-hydride elimination transition state (**TS31-P(*o*-tol)$_3$**), H−H distances between the ligand and substrate are shorter than those in **TS28-PBu$_3$** and **TS31-PBu$_3$**, revealing that the repulsive interaction between the P(*o*-tol)$_3$ ligand and substrate is greater. In fact, the ligand distortion energies $\Delta E_{dis}^{\ddagger}$(P(*o*-tol)$_3$) for the four transition states range from 1.8 to 5.5 kcal/mol, suggesting that the ligand suffers evident compression from the substrate. The introduction of $R_1$ = $CO_2Me$ exhibits the opposite effect on the distortion energy of **TS28** and **TS31**: the $\Delta E_{dis}^{\ddagger}$(P(*o*-tol)$_3$) of **TS28** increases by 0.5 kcal/mol, whereas, in the case of **TS31**, $\Delta E_{dis}^{\ddagger}$(P(*o*-tol)$_3$) reduces from 5.5 to 4.4 kcal/mol.

The presence of the substituent $R_1$ = $CO_2Me$ in **TS28-P(*o*-tol)$_3$** has three effects which increase the energy barrier of the C−C reductive elimination: (a) the repulsion between Ni and $R_1$ = $CO_2Me$ which is shown by the increment of Ni−C bond length from 1.95 to 2.09 Å, (b) the reduction of the NBO charge of C3 atoms from −0.43|e| to −0.32|e|, and (c) the substrate−ligand repulsion reflected by the short H−H distances and ligand distortion energy. In the case of **TS31-P(*o*-tol)$_3$**, the ligand suffers greater repulsion from the substrate. The H−H distances are much shorter in **TS31-P(*o*-tol)$_3$** than those in **TS28-P(*o*-tol)$_3$**. In particular, the distance between C3−H and the ligand is 2.21 Å in **TS31-*b*-P(*o*-tol)$_3$**. More interestingly, the distance between the transferred H and ligand in **TS31-d-P(*o*-tol)$_3$** is only 1.99 Å. This can explain why the ligand distortion energy in **TS31-P(*o*-tol)$_3$** is larger than those in **TS28-P(*o*-tol)$_3$**. The $R_1$ = $CO_2Me$ in **TS31-d-P(*o*-tol)$_3$** dismisses the repulsion between C3−H and the ligand, introduces new O−H attraction (2.40 Å), and lowers the ligand distortion energy from 5.5 to 4.4 kcal/mol. The reduction of the ligand distortion energy and substrate−ligand repulsion decreases the energy barrier of **TS31-d-P(*o*-tol)$_3$**. The combination of both steric and electronic effects can reduce the energy difference between **TS31** and **TS28** from 12.1 to 1.5 kcal/mol but does not alter the selectivity.



DOI: 10.1021/acs.joc.6b02957
J. Org. Chem. 2017, 82, 2150−2159

It is found from Figures 7 and 8 that the difference between the ligand distortion energies of **TS28** and **TS31** for reaction system **d** is similar for two different ligands. The ligand of **TS31-d-PBu$_3$** is 1.8 kcal/mol more distorted than that of **TS28-d-PBu$_3$** while the ligand distortion energy in **TS28-d-P(*o*-tol)$_3$** is 2.1 kcal/mol lower than that in **TS31-d-P(*o*-tol)$_3$**. However, **TS31-d-PBu$_3$** is preferred over **TS28-d-PBu$_3$**, whereas **TS31-d-P(*o*-tol)$_3$** is disfavored by 1.5 kcal/mol. This result is attributed to the different substrate−ligand repulsive interactions in **TS31-d-PBu$_3$** and **TS31-d-P(*o*-tol)$_3$**. The distance between the transferred H and ligand is taken as an index. Figure 8 depicts that the distance between the transferred H and ligand is as short as 1.99 Å in **TS31-d-P(*o*-tol)$_3$**, which indicates the strong substrate−ligand repulsion and thereby significantly increases the energy barrier of $\beta$-hydride elimination. On the other hand, the $PBu_3$ ligand adjusts its configuration from $C_{3v}$ to $C_{2v}$ in **TS31-d-PBu$_3$** and reduces the substrate−ligand repulsion, which is reflected by the H−H distance (2.47 Å) between the transferred H and ligand in Figure 7.

## CONCLUSIONS

The reaction mechanism, ligand-controlled selectivity, and origins of the regio- and stereoselectivity of Ni-catalyzed (2 + 2 + 2) cycloadditions and alkenylative cyclizations of 1,6-ene−allenes and alkenes were theoretically elucidated based on density functional calculations. The preferred catalytic cycle involves intermolecular oxidative coupling of ene−allenes and alkenes and subsequent concerted 1,4-addition via a six-membered cyclic transition state to afford a metallacycloheptane intermediate, which are the regioselectivity- and stereoselectivity-determining steps. Subsequent C−C reductive elimination leads to the cyclohexane product, whereas $\beta$-hydride elimination leads to the *trans*-diene product. The selectivity between (2 + 2 + 2) cycloaddition and alkenylative cyclization is determined to a remarkable extent by the electronic and steric factors of the ligand and substrate. With the $PBu_3$ ligand, $R_1$ substituents such as $CO_2Me$ and $CO_2tBu$ destabilize the C−C reductive elimination pathway, giving rise to the alkenylative cyclization reaction, which is attributed to the electronic and steric effects of the $R_1$ substituent. Irrespective of the nature of substituents $R_1$ and $R_2$, the C−C reductive elimination is always preferred over $\beta$-hydride elimination with the P(*o*-tol)$_3$ ligand, leading to the cyclohexane product.

## ASSOCIATED CONTENT

### Supporting Information

The Supporting Information is available free of charge on the ACS Publications website at DOI: 10.1021/acs.joc.6b02957.

Test calculations on computational methods, energy barriers of transition states **TS28** and **TS31** in Table 2, test calculations on the intermolecular oxidative coupling with the $PPh_3$ ligand, intrinsic reaction coordinate (IRC) calculations on the transition state **TS27**, test calculations on the water-assisted $\beta$-hydride elimination transition state, possible intramolecular and intermolecular $\pi-\pi$ oxidative coupling of **14** and **16**, and Cartesian coordinates (PDF)

## AUTHOR INFORMATION


### Corresponding Authors

*E-mail: yang@ims.ac.jp.
*E-mail: ehara@ims.ac.jp.

### ORCID

Tao Yang: 0000-0003-1634-6025


### Notes

The authors declare no competing financial interest.

## ACKNOWLEDGMENTS

This work was supported by a MEXT (Ministry of Education Culture, Sports, Science and Technology in Japan) program "Elements Strategy Initiative to Form Core Research Center". The computations were partially performed at the Research Center for Computational Science, Okazaki, Japan.

## REFERENCES


(1) (a) Inglesby, P. A.; Evans, P. A. *Chem. Soc. Rev.* **2010**, *39*, 2791−2805. (b) Nakamura, I.; Yamamoto, Y. *Chem. Rev.* **2004**, *104*, 2127−2198. (c) Saito, S.; Yamamoto, Y. *Chem. Rev.* **2000**, *100*, 2901−2915. (d) Lledó, A.; Pla-Quintana, A.; Roglans, A. *Chem. Soc. Rev.* **2016**, *45*, 2010−2023.

(2) (a) Domínguez, G.; Pérez-Castells, J. *Chem. - Eur. J.* **2016**, *22*, 6720−6739. (b) Amatore, M.; Aubert, C. *Eur. J. Org. Chem.* **2015**, *2015*, 265−286. (c) Domínguez, G.; Pérez-Castells, J. *Chem. Soc. Rev.* **2011**, *40*, 3430−3444. (d) Tanaka, K. *Chem. - Asian J.* **2009**, *4*, 508−518. (e) Chopade, P. R.; Louie, J. *Adv. Synth. Catal.* **2006**, *348*, 2307−2327. (f) Kotha, S.; Brahmachary, E.; Lahiri, K. *Eur. J. Org. Chem.* **2005**, *2005*, 4741−4767. (g) Varela, J. A.; Saá, C. *Chem. Rev.* **2003**, *103*, 3787−3801.

(3) (a) Geny, A.; Gaudrel, S.; Slowinski, F.; Amatore, M.; Chouraqui, G.; Malacria, M.; Aubert, C.; Gandon, V. *Adv. Synth. Catal.* **2009**, *351*, 271−275. (b) Hilt, G.; Paul, A.; Harms, K. *J. Org. Chem.* **2008**, *73*, 5187−5190. (c) Geny, A.; Leboeuf, D.; Rouquie, G.; Vollhardt, K. P. C.; Malacria, M.; Gandon, V.; Aubert, C. *Chem. - Eur. J.* **2007**, *13*, 5408−5425 and reference cited therein.

(4) (a) Kumar, R.; Tokura, H.; Nishimura, A.; Mori, T.; Hoshimoto, Y.; Ohashi, M.; Ogoshi, S. *Org. Lett.* **2015**, *17*, 6018−6021. (b) Noucti, N. N.; Alexanian, E. J. *Angew. Chem., Int. Ed.* **2013**, *52*, 8424−8427. (c) Miura, T.; Morimoto, M.; Murakami, M. *J. Am. Chem. Soc.* **2010**, *132*, 15836−15838. (d) Seo, J.; Chui, H. M. P.; Heeg, M. J.; Montgomery, J. *J. Am. Chem. Soc.* **1999**, *121*, 476−477 and reference cited therein.

(5) (a) Alvarez, S.; Medina, S.; Domínguez, G.; Pérez-Castells, J. *J. Org. Chem.* **2015**, *80*, 2436−2442. (b) Varela, J. A.; Saá, C. *J. Organomet. Chem.* **2009**, *694*, 143−149. (c) García-Rubín, S.; Varela, J. A.; Castedo, L.; Saá, C. *Chem. - Eur. J.* **2008**, *14*, 9772−9778. (d) Tanaka, D.; Sato, Y.; Mori, M. *J. Am. Chem. Soc.* **2007**, *129*, 7730. (e) Varela, J. A.; Rubín, S. G.; González-Rodríguez, C.; Castedo, L.; Saá, C. *J. Am. Chem. Soc.* **2006**, *128*, 9262−9263. (f) Yamamoto, Y.; Kinpara, K.; Saigoku, T.; Takagishi, H.; Okuda, S.; Nishiyama, H.; Itoh, K. *J. Am. Chem. Soc.* **2005**, *127*, 605−613 and reference cited therein.

(6) (a) Sakashita, K.; Shibata, Y.; Tanaka, K. *Angew. Chem., Int. Ed.* **2016**, *55*, 6753−6757. (b) Ohta, Y.; Yasuda, S.; Yokogawa, Y.; Kurokawa, K.; Mukai, C. *Angew. Chem., Int. Ed.* **2015**, *54*, 1240−1244. (c) Sakashita, K.; Masutomi, K.; Noguchi, K.; Tanaka, K. *Chem. Lett.* **2014**, *43*, 1260−1262. (d) Haraburda, E.; Torres, O.; Parella, T.; Solà, M.; Pla-Quintana, A. *Chem. - Eur. J.* **2014**, *20*, 5034−5045. (e) Dachs, A.; Pla-Quintana, A.; Parella, T.; Solà, M.; Roglans, A. *Chem. - Eur. J.* **2011**, *17*, 14493−14507. (f) Brusoe, A. T.; Alexanian, E. J. *Angew. Chem., Int. Ed.* **2011**, *50*, 6596−6600. (g) Brusoe, A. T.; Edwankar, R. V.; Alexanian, E. J. *Org. Lett.* **2012**, *14*, 6096−6099 and reference cited therein.

(7) (a) Zhou, P.; Zheng, M. F.; Jiang, H. F.; Li, X. W.; Qi, C. R. *J. Org. Chem.* **2011**, *76*, 4759−4763. (b) Shen, Y. X.; Jiang, H. F.; Chen,




DOI: 10.1021/acs.joc.6b02957
*J. Org. Chem.* 2017, 82, 2150−2159

Z. W. *J. Org. Chem.* **2010**, *75*, 1321−1324. (c) Jayanth, T. T.; Jeganmohan, M.; Cheng, C. H. *J. Org. Chem.* **2004**, *69*, 8445−8450. (d) Trost, B. M.; Tanoury, G. J. *J. Am. Chem. Soc.* **1987**, *109*, 4753−4755. (e) Brown, L. D.; Itoh, K.; Suzuki, H.; Hirai, K.; Ibers, J. A. *J. Am. Chem. Soc.* **1978**, *100*, 8232−8238. (f) Suzuki, H.; Itoh, K.; Ishii, Y.; Simon, K.; Ibers, J. A. *J. Am. Chem. Soc.* **1976**, *98*, 8494−8500.

(8) (a) Faustino, H.; Varela, I.; Mascarenas, J. L.; Lopez, F. *Chem. Sci.* **2015**, *6*, 2903−2908. (b) Obradors, C.; Echavarren, A. M. *Chem. - Eur. J.* **2013**, *19*, 3547−3551. (c) Huple, D. B.; Liu, R. S. *Chem. Commun.* **2012**, *48*, 10975−10977. (d) Dateer, R. B.; Shaibu, B. S.; Liu, R. S. *Angew. Chem., Int. Ed.* **2012**, *51*, 113−117. (e) Hernandez-Diaz, C.; Rubio, E.; Gonzalez, J. M. *Eur. J. Org. Chem.* **2016**, *2016*, 265−269.

(9) Masutomi, K.; Sakiyama, N.; Noguchi, K.; Tanaka, K. *Angew. Chem., Int. Ed.* **2012**, *51*, 13031−13035.

(10) DFT calculations have been widely used to study the transition-metal catalyzed chemical reactions; please see: (a) Cheng, G. J.; Zhang, X. H.; Chung, L. W.; Xu, L. P.; Wu, Y.-D. *J. Am. Chem. Soc.* **2015**, *137*, 1706−1725. (b) Zhang, X.; Chung, L. W.; Wu, Y.-D. *Acc. Chem. Res.* **2016**, *49*, 1302−1310.

(11) (a) Becke, A. D. *J. Chem. Phys.* **1993**, *98*, 5648−5652. (b) Lee, C. T.; Yang, W. T.; Parr, R. G. *Phys. Rev. B: Condens. Matter Mater. Phys.* **1988**, *37*, 785−789. (c) Becke, A. D. *Phys. Rev. A: At., Mol., Opt. Phys.* **1988**, *38*, 3098−3100.

(12) Hay, P. J.; Wadt, W. R. *J. Chem. Phys.* **1985**, *82*, 299−310.

(13) Zhao, Y.; Truhlar, D. G. *Theor. Chem. Acc.* **2008**, *120*, 215−241.

(14) Perdew, J. P. *Phys. Rev. B: Condens. Matter Mater. Phys.* **1986**, *33*, 8822−8824.

(15) Chai, J. D.; Head-Gordon, M. *Phys. Chem. Chem. Phys.* **2008**, *10*, 6615−6620.

(16) (a) Schwabe, T.; Grimme, S. *Phys. Chem. Chem. Phys.* **2007**, *9*, 3397−3406. (b) Schwabe, T.; Grimme, S. *Phys. Chem. Chem. Phys.* **2006**, *8*, 4398−4401.

(17) Dolg, M.; Wedig, U.; Stoll, H.; Preuss, H. *J. Chem. Phys.* **1987**, *86*, 866−872.

(18) Marenich, A. V.; Cramer, C. J.; Truhlar, D. G. *J. Phys. Chem. B* **2009**, *113*, 6378−6396.

(19) (a) Grimme, S.; Ehrlich, S.; Goerigk, L. *J. Comput. Chem.* **2011**, *32*, 1456−1465. (b) Grimme, S.; Antony, J.; Ehrlich, S.; Krieg, H. *J. Chem. Phys.* **2010**, *132*, 154104. (c) Grimme, S. *J. Comput. Chem.* **2006**, *27*, 1787−1799. (d) Grimme, S. *J. Comput. Chem.* **2004**, *25*, 1463−1473.

(20) Adamo, C.; Barone, V. *J. Chem. Phys.* **1998**, *108*, 664−675.

(21) Glendening, E. D.; Reed, A. E.; Carpenter, J. E.; Weinhold, F. *NBO*, version 3.1; University of Wisconsin: Madison, WI, 1996.

(22) Frisch, M. J.; Trucks, G. W.; Schlegel, H. B.; Scuseria, G. E.; Robb, M. A.; Cheeseman, J. R.; Scalmani, G.; Barone, V.; Mennucci, B.; Petersson, G. A.; Nakatsuji, H.; Caricato, M.; Li, X.; Hratchian, H. P.; Izmaylov, A. F.; Bloino, J.; Zheng, G.; Sonnenberg, J. L.; Hada, M.; Ehara, M.; Toyota, K.; Fukuda, R.; Hasegawa, J.; Ishida, M.; Nakajima, T.; Honda, Y.; Kitao, O.; Nakai, H.; Vreven, T.; Montgomery, J. A., Jr.; Peralta, J. E.; Ogliaro, F.; Bearpark, M.; Heyd, J. J.; Brothers, E.; Kudin, K. N.; Staroverov, V. N.; Keith, T.; Kobayashi, R.; Normand, J.; Raghavachari, K.; Rendell, A.; Burant, J. C.; Iyengar, S. S.; Tomasi, J.; Cossi, M.; Rega, N.; Millam, J. M.; Klene, M.; Knox, J. E.; Cross, J. B.; Bakken, V.; Adamo, C.; Jaramillo, J.; Gomperts, R.; Stratmann, R. E.; Yazyev, O.; Austin, A. J.; Cammi, R.; Pomelli, C.; Ochterski, J. W.; Martin, R. L.; Morokuma, K.; Zakrzewski, V. G.; Voth, G. A.; Salvador, P.; Dannenberg, J. J.; Dapprich, S.; Daniels, A. D.; Farkas, O.; Foresman, J. B.; Ortiz, J. V.; Cioslowski, J.; Fox, D. J. *Gaussian 09*, Revision B.01; Gaussian, Inc.; Wallingford, CT, 2010.

(23) Legault, C. Y. *CYLView*, 1.0b; Universitéde Sherbrooke: Canada, 2009; http://www.cylview.org.

(24) The $PMe_3$ ligand was employed as a model ligand in the mechanism calculations. Further test calculations with $P(o\text{-tol})_3$ and $PBu_3$ ligands were performed on **TS19** and **TS25**. **TS19** is more than 20 kcal/mol higher in energy than **TS23**, in agreement with calculations with the model ligand.

(25) (a) Liu, P.; McCarren, P.; Cheong, P. H. Y.; Jamison, T. F.; Houk, K. N. *J. Am. Chem. Soc.* **2010**, *132*, 2050−2057. (b) McCarren, P. R.; Liu, P.; Cheong, P. H. Y.; Jamison, T. F.; Houk, K. N. *J. Am. Chem. Soc.* **2009**, *131*, 6654−6655.

(26) Besides the internal allene−alkene oxidative coupling **TS21** which gives rise to [5,5]-bicyclic intermediate **22**, the intramolecular external-allene−alkene oxidative couplings which lead to [6,5]-bicyclic intermediates were also calculated. Even though they have low energy barriers of about 24 kcal/mol, those TSs could not compete with **TS25** when $R_2$ substitution is introduced as in the case of reaction system **b**, since the energy barriers of **TS25-b** decrease to about 20 kcal/mol. Please see Table 1 and Supporting Information for details.

(27) Kozuch, S.; Shaik, S. *Acc. Chem. Res.* **2011**, *44*, 101−110.

(28) (a) Komagawa, S.; Wang, C.; Morokuma, K.; Saito, S.; Uchiyama, M. *J. Am. Chem. Soc.* **2013**, *135*, 14508−14511. (b) Hong, X.; Liu, P.; Houk, K. N. *J. Am. Chem. Soc.* **2013**, *135*, 1456−1462.

(29) Possible intermolecular alkene−internal allene and alkene−alkene oxidative couplings were also examined, but their energy barriers are higher than 55 kcal/mol. Please see Supporting Information for details.

(30) Huang, G.; Kalek, M.; Himo, F. *J. Am. Chem. Soc.* **2013**, *135*, 7647−7659.

(31) The intramolecular alkene−alkene oxidative coupling can take place under some conditions. For example, Noucti and Alexanian very recently reported an experimental Ni-catalyzed intramolecular (2 + 2) cycloaddition of 1,6-ene-allenes with both mono- and bidentate phosphine ligands; see: Noucti, N. N.; Alexanian, E. J. *Angew. Chem., Int. Ed.* **2015**, *54*, 5447−5450. The test calculations on the Ni-catalyzed (2 + 2) cycloaddition also theoretically confirmed that the intramolecular oxidative coupling of 1,6-ene-allenes could occur. However, once the alkene exists, the intermolecular oxidative coupling will be preferred over the intramolecular oxidative coupling. Please see the Supporting Information for more details.

(32) In 2010, González and co-workers reported thermally induced intramolecular (2 + 2 + 2) cycloadditions of macrocyclic triynes and enediynes. They found that the energy barrier of $\beta$-hydride transfer can be significantly lowered when assisted by a water molecule. Please see: González, I.; Pla-Quintana, A.; Roglans, A.; Dachs, A.; Solà, M.; Parella, T.; Farjas, J.; Roura, P.; Lloveras, V.; Vidal-Gancedoe, J. *Chem. Commun.* **2010**, *46*, 2944−2946. We tried to locate a water molecule-assisted transition state based on **TS31** but the water molecule prefers to be adsorbed on the Ni atom or the energy barrier of water-assisted TS is higher than 55 kcal/mol. Please see the Supporting Information for details.

(33) Dahy, A. A.; Koga, N. *Organometallics* **2015**, *34*, 4965−4974.

(34) Stockis, A.; Hoffmann, R. *J. Am. Chem. Soc.* **1980**, *102*, 2952−2962.

(35) (a) Yang, T.; Nagase, S.; Akasaka, T.; Poblet, J. M.; Houk, K. N.; Ehara, M.; Zhao, X. *J. Am. Chem. Soc.* **2015**, *137*, 6820−6828. (b) Yang, T.; Zhao, X.; Nagase, S. *J. Comput. Chem.* **2013**, *34*, 2223−2232.

(36) Stegmuller, A.; Tonner, R. *Inorg. Chem.* **2015**, *54*, 6363−6372.



DOI: 10.1021/acs.joc.6b02957
*J. Org. Chem.* 2017, 82, 2150−2159